Molecular Order Affects Interfacial Water Structure and Temperature-Dependent Hydrophobic Interactions between Nonpolar Self-Assembled Monolayers

Bradley C. Dallin[1], Hongseung Yeon[1], Alexis R. Ostwalt[2], Nicholas L. Abbott[1,3], and Reid C. Van Lehn[1]*

1) Department of Chemical and Biological Engineering, University of Wisconsin – Madison, 1415 Engineering Drive, Madison, WI, 53706 USA
2) Department of Chemical and Biological Engineering, Montana State University, 306 Cobleigh Hall, Bozeman, MT 59715 USA
3) Department of Chemical and Biomolecular Engineering, Cornell University, 120 Olin Hall, Ithaca, NY, 14853

*send correspondence to: vanlehn@wisc.edu

Abstract

Understanding how material properties affect hydrophobic interactions—the water-mediated interactions that drive the association of nonpolar materials—is vital to the design of materials in contact with water. Conventionally, the magnitude of the hydrophobic interactions between extended interfaces is attributed to interfacial chemical properties, such as the amount of nonpolar solvent-exposed surface area. However, recent experiments have demonstrated that the hydrophobic interactions between uniformly nonpolar self-assembled monolayers (SAMs) also depend on molecular-level SAM order. In this work, we use atomistic molecular dynamics simulations to investigate the relationship between SAM order, water structure, and hydrophobic interactions to explain these experimental observations. The SAM-SAM hydrophobic interactions calculated from the simulations increase in magnitude as SAM order increases, matching experimental observations. We explain this trend by showing that the molecular-level order of the SAM impacts the nanoscale structure of interfacial water molecules, leading to an increase in water structure near disordered SAMs. These findings are consistent with a decrease in the solvation entropy of disordered SAMs, which is confirmed by measuring the temperature dependence of hydrophobic interactions using both simulations and experiments. This study elucidates how hydrophobic interactions can be influenced by an interfacial physical property, which may guide the design of synthetic materials with fine-tuned interfacial hydrophobicity.

Introduction

In aqueous environments, nonpolar materials experience attractive, water-mediated hydrophobic interactions that drive a range of behaviors relevant to biological and synthetic materials, including the folding and misfolding of proteins,[1-3] the self-assembly of colloidal particles,[4-5] the recognition of nonpolar domains on protein substrates,[6-9] and the surface adsorption of proteins and nanoparticles.[10-13] The broad relevance of these interactions has inspired significant research efforts relating hydrophobic interactions to the nanoscale structure of water.[14-33] For nonpolar solutes, qualitative differences in water structure are identified at two limiting length scales.[14, 16, 34] The hydration of a small nonpolar solute with a radius less than ~1 nm leads to the reorganization of water molecules to form a structured, clathrate-like shell around the solute that maintains a favorable hydrogen bonding network.[34] Conversely, the hydration of a large nonpolar solute with a radius greater than ~1 nm, including a macroscopic surface, results in broken hydrogen bonds and the creation of an interface resembling that between liquid and vapor.[16, 23] As a result, the solvation free energy of a small nonpolar solute (*i.e.*, the free energy penalty for inserting the nonpolar solute into water) scales with solute volume, the solvation entropy is negative, and the association of two small solutes is weakly favorable and entropically driven. Conversely, the solvation free energy of a large nonpolar solute scales with the solute surface area, the solvation entropy is positive, and the association of two large solutes is highly favorable and enthalpically driven.

This molecular description of hydrophobic hydration has been valuable for predicting hydrophobic interactions between idealized nonpolar solutes and has inspired estimates of hydrophobic interactions in more complex systems. For example, hydrophobic driving forces relevant to protein folding or interactions with lipid bilayer membranes are often estimated based on the solvent-accessible surface area (SASA) of a solute because hydrophobic interactions scale with surface area in the large length scale limit.[35-38] However, the diverse physical and chemical properties of materials surfaces can confound predictions of hydrophobic interactions with systems that significantly differ from idealized nonpolar solutes.[39-43] For example, experiments have shown that polar or charged moieties near nonpolar regions of a substrate can dramatically influence hydrophobic interactions, complicating simple estimates of these interactions based on the SASA alone.[41-42] These findings suggest that spatially varying chemical properties can affect the measurements of hydrophobic interactions and illustrates the complexity associated with predicting hydrophobic interactions at realistic materials interfaces.

In addition to interfacial chemical properties, interfacial physical properties can also affect hydrophobic interactions. In a recent experimental study, we quantified the hydrophobic force between two self-assembled monolayers (SAMs) by measuring the adhesion force between a SAM-functionalized atomic force microscope (AFM) tip and a SAM-functionalized planar gold substrate. Both the AFM and substrate SAMs were composed of uniformly nonpolar alkanethiol ligands with a varying number of methylene groups (*i.e.,* ligand chain length) and degree of saturation. The hydrophobic force was determined by calculating the difference between the adhesion force measured in aqueous triethanolamine (TEA) and in methanol. It was observed that the magnitude of the hydrophobic force increased as a function of the ligand chain length, indicating that SAMs with long, quasi-crystalline ligands appeared more hydrophobic than SAMs with short, disordered ligands.[43] A similar trend was also identified from recent experimental measurements of hydrophobic interactions between air bubbles and nonpolar SAMs.[44] This surprising result suggests that surfaces that may be considered "idealized" large length scale nonpolar solutes may still have variable hydrophobic interactions related to SAM physical properties. Both sets of experiments, however, lacked the ability to explore the atomistic details of the SAM-water interface to explain why hydrophobic interactions between nonpolar SAMs depends on molecular-level ligand order.

In this work, we performed joint simulation and experimental studies to investigate the molecular details of the SAM-water interface and to relate ligand order, interfacial water structure, and interfacial hydrophobicity. We hypothesize that water molecules at a disordered SAM interface partially exhibit the structure of water molecules around small nonpolar solutes, causing a disordered SAM to appear less hydrophobic than an ordered SAM. To investigate this hypothesis, we developed a classical molecular dynamics (MD) simulation approach that qualitatively reproduces our previous experimental observation that hydrophobic interactions increase as a function of SAM order.[43] We then characterized water structure

by quantifying the orientation of interfacial water molecules and the preference for fully satisfying a hydrogen bonding network. Based on these measurements, we predicted that the increase in water structure at the disordered SAM surface would reduce its solvation entropy relative to an ordered SAM surface. We confirmed our predictions using MD simulations and AFM experiments by measuring the hydrophobic interactions as a function of temperature. These findings provide insight into the effect of interfacial physical properties on hydrophobic interactions, enabling new design rules for fine-tuning hydrophobic interactions with functionalized materials.

Materials and Methods

A detailed description of the simulation and experimental procedures is included in the Supporting Information (Sections S1 and S4); here only key methodological details are provided.

Simulations

Isolated SAM system.

An isolated SAM system was used to study the SAM order parameters and interfacial water structure at the SAM surface. Each SAM was constructed from alkanethiol ligand chains with the chemical formula $CH_3(CH_2)_nSH$, where the number of methylene groups, n, ranged from 3 to 17. The sulfur atoms were restrained to locations consistent with their positions on a gold (111) lattice.[45] Gold atoms were not explicitly included in the simulations; additional discussion regarding the influence of gold is included in SI Section S1. The OPLS-AA force field reparametrized for long hydrocarbons (LOPLS-AA)[46] was used to model the interactions of the atoms in the SAMs. 128 alkanethiol ligand chains were included (64 in each SAM), spanning an area of 3.46×4.00 nm^2, with 5 nm of water positioned between the methyl terminated ends of the two SAMs. Water molecules were modeled with the modified TIP3P model, which has been shown to accurately reproduce hydration free energies in conjunction with the LOPLS-AA force field.[46-47] Additional discussion and simulations demonstrating the effect of the water model and force field are included in SI Section S1. Molecular dynamics simulations were performed with the simulation package GROMACS (version 2016.1)[48] using a 2-fs timestep. The pressure was maintained at 1 bar using an anisotropic Parrinello-Rahman barostat[49] and the temperature was maintained at 300 K using a velocity rescaling thermostat.[50] Each simulation was comprised of two parts: 5 ns of equilibration to relax the SAM layers followed by 20 ns of production. System configurations were sampled every 1 ps. Error bars were calculated by taking the standard deviation between the measurements performed for the top and bottom SAM surfaces.

Simulated AFM-like SAM system.

The AFM-like SAM system was used to measure the potential of mean force (PMF) as a function of SAM-SAM separation. The system was constructed by removing the water molecules from the equilibrated isolated SAM system. The inward facing SAM system was placed in a 3D periodic box with 3 nm added in the x- and y-directions and 4 nm in the z-direction (1.5 nm on each side and 2 nm above and below) that was then solvated. The box size was larger than the SAM dimensions to allow the water molecules to retain bulk properties. Details about box size selection are included in SI Section S1. The sulfur atoms of the SAMs were restrained in the x- and y-directions using a harmonic potential and the sulfur atoms of the bottom SAM were restrained in the z-direction to maintain the alignment of the SAMs during the simulations. Additionally, all the carbon atoms in the perimeter ligands were restrained in the x- and y-directions using harmonic potentials to avoid edge effects. Umbrella sampling[51] was performed for each SAM system using 28 simulation windows and the weighted histogram analysis method (WHAM)[52] was then used to compute PMFs as a function of SAM-SAM separation. Each window was simulated for 26 ns (6 ns of equilibration and 20 ns of production). The same force field and runtime parameters used in the isolated SAM simulations were used for these simulations. The umbrella sampling simulation setup and protocol is detailed in SI Section S1.

Experiments

Materials

1-Butanethiol (*n*=3, 99%), 1-decanethiol (*n*=9, 96%), 1-dodecanethiol (*n*=11, 98%), 1-hexadecanethiol (*n*=15, 95%), 1-octadecanethiol (n=17, 98%), (Z)-octadecen-1-thiol (n=17, unsaturated) triethanolamine HCl (TEA, 99%) and methanol (anhydrous, 99.8%) were purchased from Sigma-Aldrich (Milwaukee, WI). Ethanol (Sigma-Aldrich; reagent, anhydrous, denatured or Decon Labs; anhydrous, 200 proof) was used for preparation of thiol solutions and for rinsing. The resistivity of de-ionized water used in this study was 18.2 MΩcm. All chemicals were used as received without any further purification. The AFM tips (triangular in shape, nominal spring constant of 0.1 N m^{-1}) were purchased from Bruker Nano Company (Santa Barbara, CA). Silicon wafers were purchased from Silicon Sense (Nashua, NH).

Gold deposition on AFM tips and silicon substrates

AFM tips and silicon wafers were coated sequentially with a 20 Å layer of titanium and 200 Å layer of gold at normal incidence using an electron beam evaporator (Tek-Vac Industries, Brentwood, NY). The rates of deposition of titanium and gold were controlled at ~0.2 Å/s. The pressure and temperature in the evaporator were maintained at 1.5×10^{-6} Torr and 55°C, respectively, throughout evaporation processes. Gold-coated tips and silicon wafers were used immediately after gold deposition.

Preparation of chemically functionalized AFM tips and substrates

Triangular-shaped cantilevers with nominal spring constants of 0.1 Nm^{-1} was used for all force measurements. Following deposition of the gold, the gold-coated AFM tips and Si wafers were immersed in 1 mM ethanolic solutions of either 1-butanethiol, 1-decanethiol, 1-dodecanethiol, 1-hexadecanethiol, 1-octadecanethiol or (Z)-octadecen-1-thiol and incubated overnight. Upon removal from solution, the chemically modified AFM tips were thoroughly rinsed with ethanol, dried under a stream of nitrogen, and immediately transferred to the AFM fluid cell for the force measurement.

Adhesion force measurements

Adhesion force measurements were performed using a Nanoscope IIIa Multimode AFM equipped with a fluid cell (Veeco Metrology Group, Santa Barbara, CA) and temperature-controlled stage (MultiMode Heater/Cooler, Veeco Metrology Group) with a precision of ±0.5K. The spring constants of the cantilevers were calibrated using Sader's method on a PCM-90 Spring Constant Calibration Module (Novascan Technologies, Ames, IA) and determined to be ~0.340±0.007 N m^{-1}. A past study has reported that changes in temperature between 25 and 65°C have a minor influence only on the spring constant.[53] All force measurements were performed in either 10 mM TEA in aqueous solution (at pH 7.0) or pure methanol. Dissolved gases were minimized by applying a vacuum for 1h prior to performing force measurements. We analyzed the approach curves from our AFM measurements to determine if we can detect any influence of the underlying gold substrate on the jump-in distance (Figure S13). Within the experimental uncertainty of our measurements, we do not measure a chain-length-dependence of the jump-in distance (see SI Section S5).

Unless otherwise stated, adhesion force measurements were performed by sequentially heating samples to 283K, 298K, 308K and then 318K. At each temperature, the samples were equilibrated for 10 mins prior to performing force measurements. After heating to 318K, each sample was sequentially cooled to 308K, 298K and then 283K, with adhesion force measurements performed at each temperature. For SAMs with *n*=3, the samples were not heated higher than 308K due to thermal instability of the *n*=3 SAMs. Force curves were obtained by approaching and retracting the AFM tip from the sample at a speed of 1,000 nm/s, and AFM tip and samples were held in adhesive contact for 500 μs prior to measuring pull-off forces. Adhesion forces were measured at least 1,500 times with four independently prepared samples (Table S4) and the mean adhesion forces were calculated by fitting a Gaussian curve to the histogram of adhesion forces using Origin software (OriginLab Corporation, Northampton, MA). Any histogram of forces that exhibited a non-Gaussian distribution was excluded from our analysis. The error bars presented in the

experimental results measure the standard error of the mean adhesion forces and incorporate the variation in tip geometries between independent AFM probes. The number of independent AFM tips used in experiments reported is presented in SI Section S4.

Results & Discussion

Simulations of SAM order.

To investigate the atomistic details of the SAM-water interface, we performed MD simulations to quantify molecular-level SAM order and the strength of SAM-SAM hydrophobic interactions. To represent the experimental AFM system (Figure 1A), we prepared two single-component alkanethiol SAM layers such that the methyl end groups were presented adjacent to the aqueous phase resulting in two SAM-water interfaces (Figure 1B). SAMs were modeled with alkanethiol ligands with the chemical formula $CH_3(CH_2)_nSH$, where the number of methylene groups, n, ranged from 3 to 17. Representative short (n=3) and long (n=11) alkanethiol ligands are shown in Figure 1C.

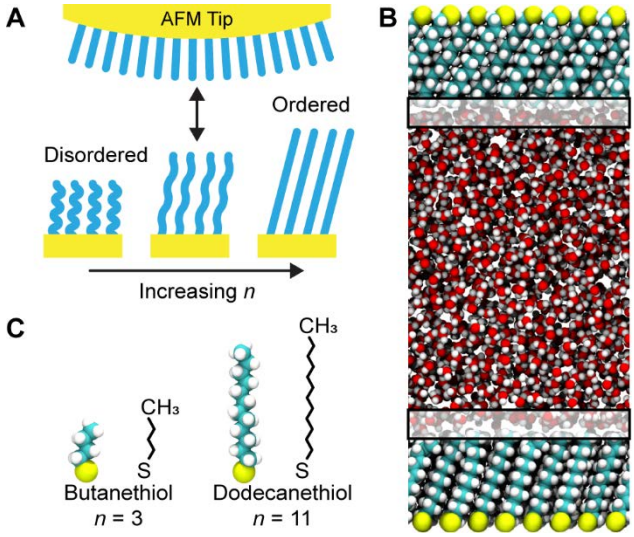

Figure 1. (A) Schematic depiction of the experimental AFM system, illustrating three distinct SAMs of increasing ligand length and ligand order. (B) Simulation snapshot of the isolated alkanethiol SAMs with n=11. Grey boxes highlight interfacial water regions. (C) Simulation representations and molecular structures of representative alkanethiol ligand chains, where n indicates the number of methylene groups in the ligand chain.

We quantified SAM order by determining the relative fraction of *trans* dihedral conformations as a function of ligand chain length (Figure 2A). Dihedral angles were calculated with respect to each carbon-carbon bond in the ligand backbones. A dihedral angle was counted as a *trans* conformer if the computed angle was between 120° and 240°. Similar metrics comparing the fraction of *trans*/*gauche* conformations have been used in simulations to characterize the structural order of lipid membranes, SAMs, and other soft materials.[54-56] A fraction of *trans* conformations near one indicates perfectly ordered ligands that pack tightly to form a quasi-crystalline structure, whereas a fraction of *trans* conformations less than one indicates disordered ligands that pack less tightly and are prone to molecular fluctuations. Figure 2A shows a sharp increase in the fraction of *trans* dihedral conformations as the ligand chain length in the SAM increases from n=5 to n=6, suggesting an order-disorder transition, followed by a gradual increase in the fraction of *trans* dihedrals for the SAMs containing longer ligands.

We also computed the fraction of *trans* dihedrals for a SAM containing (Z)-6-dodecen-1-thiol (n=11, unsaturated) ligands. The double bond in this ligand is expected to disrupt packing relative to a SAM containing saturated ligands with the same number of methylene groups. The *cis* double bond was excluded in this calculation to directly compare to the SAMs containing saturated ligands. As expected, we observed

a decrease in the fraction of *trans* conformations for the unsaturated n=11 SAM (grey square in Figure 2A) compared to the saturated n=11 SAM. We further characterized SAM order with other parameters, including the root-mean-square fluctuations of SAM ligands, the hexatic order parameter, and the variance of SAM height (Figure S8). These measurables also show signatures of an order-disorder transition and agree with the trend that molecular-level order increases with increasing ligand chain length and saturation.

The simulation results are consistent with our prior experimental measurements of C-H asymmetric stretching modes (reproduced in Figure 2B).[43] In the experiments, the detected wavenumber decreased from values consistent with liquid-like to crystalline-like packing as a function of ligand chain length, indicating an increase in the order of the SAMs. The experiments also found that a SAM containing unsaturated ligands is less ordered than a SAM containing saturated ligands with the same number of methylene groups (blue circle in Figure 2B). Compared to the simulations, the experimental measurements identify a less abrupt change in order between n=5 and n=6 and the order parameter does not plateau to the extent observed in the simulations. However, we note that the simulation representation of the SAMs is idealized and lacks features of the experimental system that could affect SAM order, such as packing defects, grain boundaries, or substrate roughness. Figure S9 shows that randomly removing ligands from the SAM (*i.e.*, introducing simple point defects) resulted in a decreased fraction of *trans* conformations for the ordered SAMs (n=7 and n=11), while adding point defects to the disordered SAM (n=3), did not significantly affect SAM order. We further calculated the fraction of *trans* dihedrals as a function of ligand chain length for SAMs with

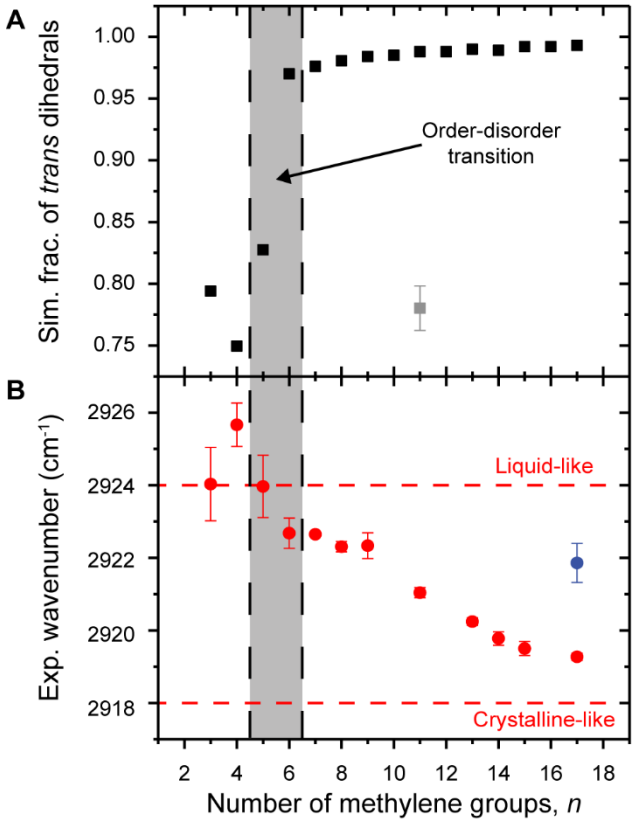

Figure 2. Measurements of SAM order. (A) Fraction of *trans* dihedrals as a function of ligand chain length measured with simulations. The SAM containing unsaturated ligands is indicated by the grey square. The grey region between the dashed lines indicates the apparent order-disorder transition. Error bars report the standard deviation from the mean value measured for the top and bottom surfaces. Error bars not seen are smaller than the symbols. (B) Asymmetric C-H stretching wavenumber as a function of ligand chain length measured with polarization−modulation infrared reflection−adsorption spectroscopy. Data are reproduced from Ref. 43. The dashed horizontal red lines indicate the change from liquid-like to crystalline-like SAMs with increasing ligand chain length.[57] The SAM containing unsaturated ligands is indicated by the blue circle.

10% of the ligands removed and observed a gradual increase in SAM order that similar to the experimental observations (Figure S9). These results suggest that the broader transition observed in the experiments may be due to the presence of packing defects that primarily affect more ordered SAMs, leading to a less abrupt change in SAM order compared to the simulations of perfect SAMs. We conclude that the simulations and experiments show reasonable qualitative agreement subject to the differences between the systems, supporting the argument that ligand chain length and saturation affect SAM order.

Simulations of hydrophobic interactions between SAMs.

We next developed a simulation system to mimic the experimental approach for measuring hydrophobic interactions. In the experiments, the adhesion force between the AFM tip and substrate (*i.e.*, the force required to pull the AFM tip off the substrate) was first measured in aqueous TEA solution to quantify the combined effect of van der Waals, electrical double layer, and hydrophobic interactions, and then measured again in a solution containing pure methanol. Methanol is an unstructured solvent that eliminates hydrophobic interactions, but has a refractive index similar to water's and preserves similar van der Waals interactions.[43] Prior work has also concluded that electrical double layer interactions do not contribute significantly to adhesion forces between alkanethiol SAMs in water.[41, 43] The difference in the adhesion force between the measurements in aqueous TEA solution and pure methanol can thus be attributed to hydrophobic interactions[41, 43] and is expected to correlate with simulation measurements.

We simulated two alkanethiol SAMs with ligand chain lengths ranging from n=3 to n=15 that were placed in a bulk water reservoir and positioned such that the methyl end groups of each SAM make contact if the SAM-SAM separation is sufficiently decreased; SAM-SAM separation is defined as the z-component of the distance between the centers of mass of the methyl end groups in the top and bottom SAMs. PMFs as a function of SAM-SAM separation were computed as described in the Materials and Methods. Mean forces between the SAMs were obtained from the derivatives of the PMFs with respect to SAM-SAM separation (SI Section S1); positive values indicate attractive interactions. We performed an additional set of umbrella sampling simulations for the n=11 SAM in vacuum to obtain a corresponding PMF and mean force. The mean force in vacuum includes contributions from SAM-SAM interactions, including van der Waals, electrostatic, and ligand-mediated interactions at close separation, but excludes any water-mediated interactions. The mean force in vacuum was thus subtracted from the mean force in water to obtain the water-mediated force as a function of SAM-SAM separation. Figure 3A shows the mean forces computed for the n=11 SAMs in both water and vacuum and the corresponding water-mediated force (*i.e.*, their difference). The accompanying simulation snapshots indicate three regions. The first region at small SAM-SAM separation contains the maximum value of the water-mediated mean force and corresponds to the first water molecules entering the volume between the SAMs. The second region is where water molecules constantly fill the volume between the SAMs. The third region is where the volume between the SAMs becomes saturated with water and the forces between the SAMs decays to zero. We did not observe interdigitation between the ligand chains or deviations in the SAM order as a function of SAM-SAM separation (Figure S1).

We hypothesized that the maximum water-mediated force measured in the simulations would correspond to the hydrophobic force measured experimentally as indicated by the red arrow in Figure 3A. To determine the hydrophobic force for a range of SAMs, we approximated the magnitude of the mean force in vacuum at the SAM-SAM separation corresponding to the hydrophobic force by computing only the van der Waals interactions between the two SAMs, assuming that the electrostatic contribution to the mean force in vacuum is negligible because all SAMs studied are nonpolar. Because the simulations were performed with the classical LOPLS-AA force field[46] in which Lennard-Jones (LJ) and Coulomb potentials are used to model intermolecular interactions, we approximated the van der Waals interactions between the two SAMs by calculating the direct SAM-SAM LJ interactions, which capture intermolecular interactions not attributed to partial charges. Using this approximation, we found no significant difference between the hydrophobic force for the n=11 SAM calculated by subtracting only the van der Waals force (0.72±0.04 nN) or calculated by subtracting the mean force in vacuum (0.71±0.04 nN) from the mean force in water (Figure S3). This result suggests that subtracting the van der Waals force is sufficient to compute the hydrophobic

force between the SAMs. All computationally determined hydrophobic forces that we report were determined using this approximation to avoid additional PMF calculations in vacuum; additional details are provided in SI Section S1. We note that some system features, such as electronic polarization or water dissociation, are not explicitly represented in this force field; these omissions may affect quantitative comparisons with experiments but are not expected to affect qualitative trends.

Figure 3B shows the computationally determined hydrophobic force as a function of ligand chain length, while Figure 3C shows the experimentally determined hydrophobic force as a function of ligand chain length measured in previous work.[43] In both the simulations and experiments the hydrophobic force increased with ligand chain length. In the experiments, there was a sharp increase in the hydrophobic force between n=5 and n=6. The simulations identified a similar sharp increase in the hydrophobic force between n=5 and n=7, coinciding with the order-disorder transition observed in Figure 2. Both simulations and experiments also measured a weaker hydrophobic force between SAMs containing unsaturated ligands compared to the SAMs containing saturated ligands with the same number of methylene groups (grey square and blue circle in Figure 3B and Figure 3C, respectively). To compare simulation and experimental results quantitatively, we estimated the contact area in the simulations as the product of the x- and y-simulation box dimensions (13.84 nm^2). The contact area of the AFM tip and substrate has previously been estimated as 360 nm^2.[43] We normalized the hydrophobic forces by these surfaces areas and found the forces to range between 26.7 to 52.4 pN/nm^2 and 8.6 to 67.8 pN/nm^2 nm^2 for the simulations and experiments,

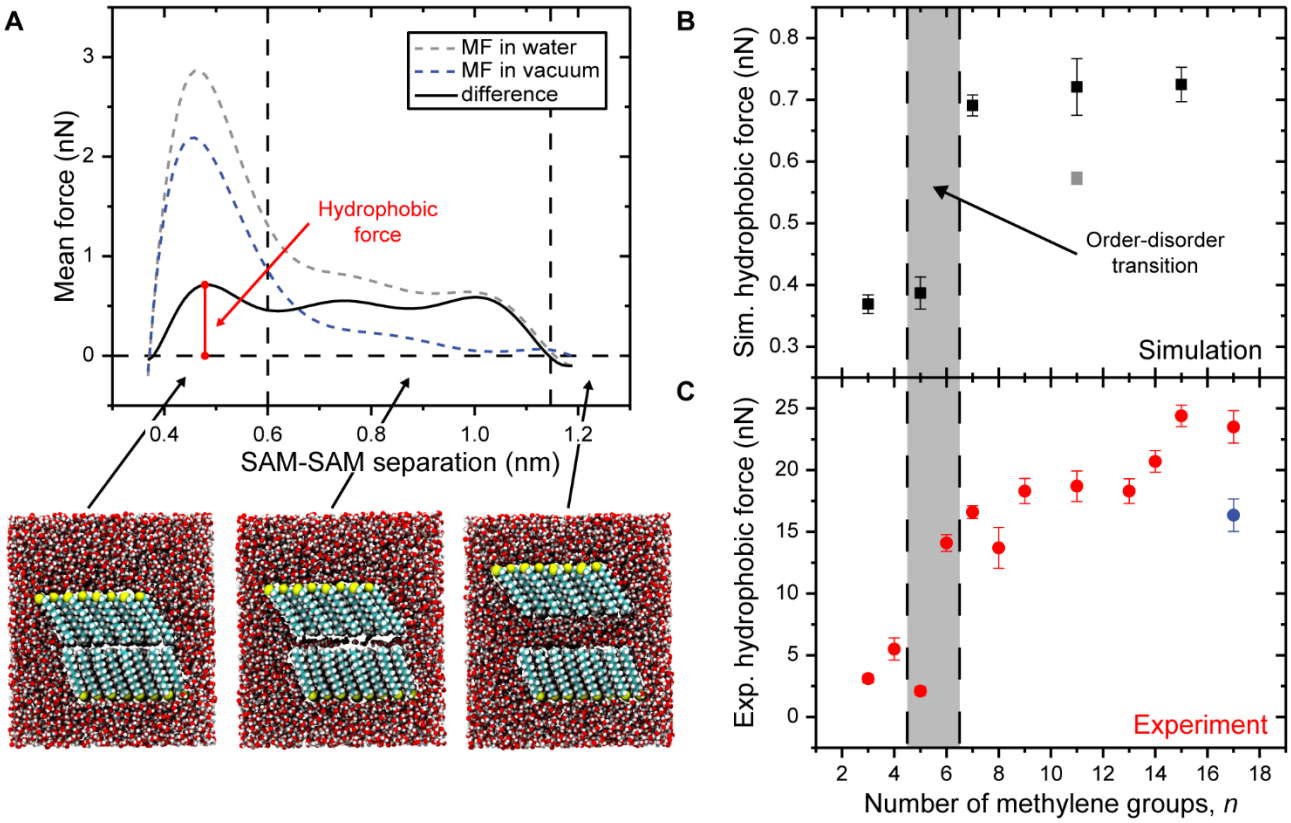

Figure 3. (A) Mean force from umbrella sampling (grey), van der Waals force (blue), and their difference (black). The hydrophobic force is indicated by the red arrow. Three simulation snapshots at different SAM-SAM separations illustrate each region of the force curve. Hydrophobic force as a function of ligand chain length measured by (B) MD simulations and (C) AFM experiments (reproduced from Ref. 43). Errors bars in (B) report the propagated standard deviation of the mean value from bootstrap analysis and block averaging for the PMF and van der Waals interaction, respectively (SI Section S1). Error bars not seen are smaller than the symbols. The grey square and blue circle are the measured hydrophobic force for the SAM containing unsaturated ligands from the simulations and experiments, respectively. The grey region between the dashed lines indicates the order-disorder transition identified in Figure 2.

respectively. While we cannot claim quantitative agreement due to the uncertainty in the AFM-substrate contact area, the simulations and experiments reproduce forces on the same order of magnitude in addition to similar qualitative trends.

The simulations presented above did not include an explicit gold substrate because including an explicit gold substrate led to poor agreement between simulated SAM order parameters and the experimental trends presented in Figure 2, as detailed in SI Section S1. Past experimental studies have reported that van der Waals forces associated with gold underlying monolayers formed from alkanethiols can influence contact angles of liquids on SAMs.[58] However, as discussed in our recent paper,[43] van der Waals forces from the gold, if dominant in our measurements of adhesion, would cause a chain-length-dependence of the adhesion force that is opposite to that found in our experiments performed in both water and methanol. We refer the reader to our prior paper[43] for a discussion of the potential role of van der Waals forces from the gold substrates in our adhesion measurements. Moreover, the difference in the hydrophobic forces observed in both simulations and experiments for SAMs with similar ligand chain lengths but varying in chain saturation (Figure 3) suggests that van der Waals forces with the gold substrate, which would be similar for these SAMs due to their similar thickness, are not dominant in our measurements. Based on these experimental observations and the good agreement between the trends observed in simulations and experiments (Figure 2 and Figure 3), we conclude that the simplified simulation system lacking gold captures similar physical behavior as observed in the experiments, prompting further analysis of the molecular-scale water structure near the interfaces to explain trends in SAM-SAM hydrophobic interactions.

Characterization of interfacial water structure as a function of ligand chain length.

We next quantified interfacial water structure as a function of ligand chain length to determine why SAM order affects hydrophobic interactions between SAMs. Each measurement was performed for the five saturated SAMs studied in Figure 3B, which were divided into two groups: disordered ligands with relatively weak hydrophobic interactions (n=3 and n=5) and ordered ligands with relatively strong hydrophobic interactions (n=7, n=11, and n=15). Measurements were performed using the isolated SAM representation presented in Figure 1B and used previously to measure SAM order. Four order parameters were measured as described below; each is presented in Figure 4 with red arrows indicating the shifts in the measurements for the disordered ligands relative to the ordered ligands.

Figure 4A shows the water density, normalized by the density of bulk water, as a function of the distance from the SAM surface projected along the surface normal (*i.e.*, the z-axis of the simulation box). We defined the SAM surface as the z-position of the center of mass of the methyl end groups. We observed similar oscillatory hydration behavior and pronounced primary and secondary hydration shells (peaks in the density profiles) for each SAM. There is a subtle increase in the width and decrease in the height of the first solvation peak for the disordered SAMs (indicated by the red arrows in Figure 4A), which suggests that water has a slight preference for the disordered SAM interface. However, the change is small, with an approximately 7% difference between the ordered and disordered SAMs, and density profiles cannot conclusively distinguish the hydrophobicity of SAM surfaces.[18] To better characterize interfacial water structure, we computed the distribution of O-H bond angles normal to the surface,[59-60] the distribution of coneighboring water triplet angles,[26, 61-62] and the distribution of the number of hydrogen bonds per water molecule. Each of these parameters was measured for only interfacial water molecules, which we defined as water molecules in a fictitious slab with the same lateral dimension as the simulation box and a 3 Å width in the z-direction. The center of the slab was placed 1.5 Å above the SAM surface and is highlighted as shaded squares at each SAM-water interface in Figure 1B.

Figure 4B shows the probability distribution of the angle, φ, between each O-H bond vector and a vector normal to the surface (normalized by 1/sin(φ) to correct for the trivial contribution of the solid angle variation); the inset in Figure 4B illustrates φ. This distribution measures the tendency for water to form dangling hydrogen bonds near hydrophobic surfaces.[59, 63] A dangling hydrogen bond is defined by an O-H bond vector that points toward the surface (φ=180°). Interfacial water molecules form dangling hydrogen bonds to optimize the hydrogen bond network by forming three hydrogen bonds with water molecules in

the bulk.[59] The probability distribution of φ at a hydrophobic surface has increased populations near 180° due to dangling hydrogen bonds and near 70° (approximately 180° minus the H-O-H bond angle) due to the other O-H bond vector pointing away from the surface. Conversely, the distribution for a hydrophilic surface has peaks at 0° and 120°. The increased population at 0° is due to the O-H bond vector pointing away from the surface and the increased population at 120° is the opposite O-H bond vector pointing toward the surface.[60] Figure 4B shows that water near each of the SAM surfaces created dangling hydrogen bonds with no preference for the disordered or ordered surface. For disordered SAMs, there is a slight depletion in the probability distribution at approximately 70°-90° and a slight enhancement at approximately 120°-140° (approximately a 4% difference between the ordered and disordered SAMs for both depletion and enhancement). These changes suggest a shift in the orientation of the O-H bond vector opposite of the dangling hydrogen bond from satisfying hydrogen bonds with the bulk water to a slight affinity toward the surface. Similar shifts have been observed in the probability distributions of water molecules near silica surfaces with increasing hydrophilicity.[60]

Figure 4C shows the probability distribution of the water triplet angle, θ, which is defined as the angle formed between the oxygen atom of an interfacial water molecule and the oxygen atoms of

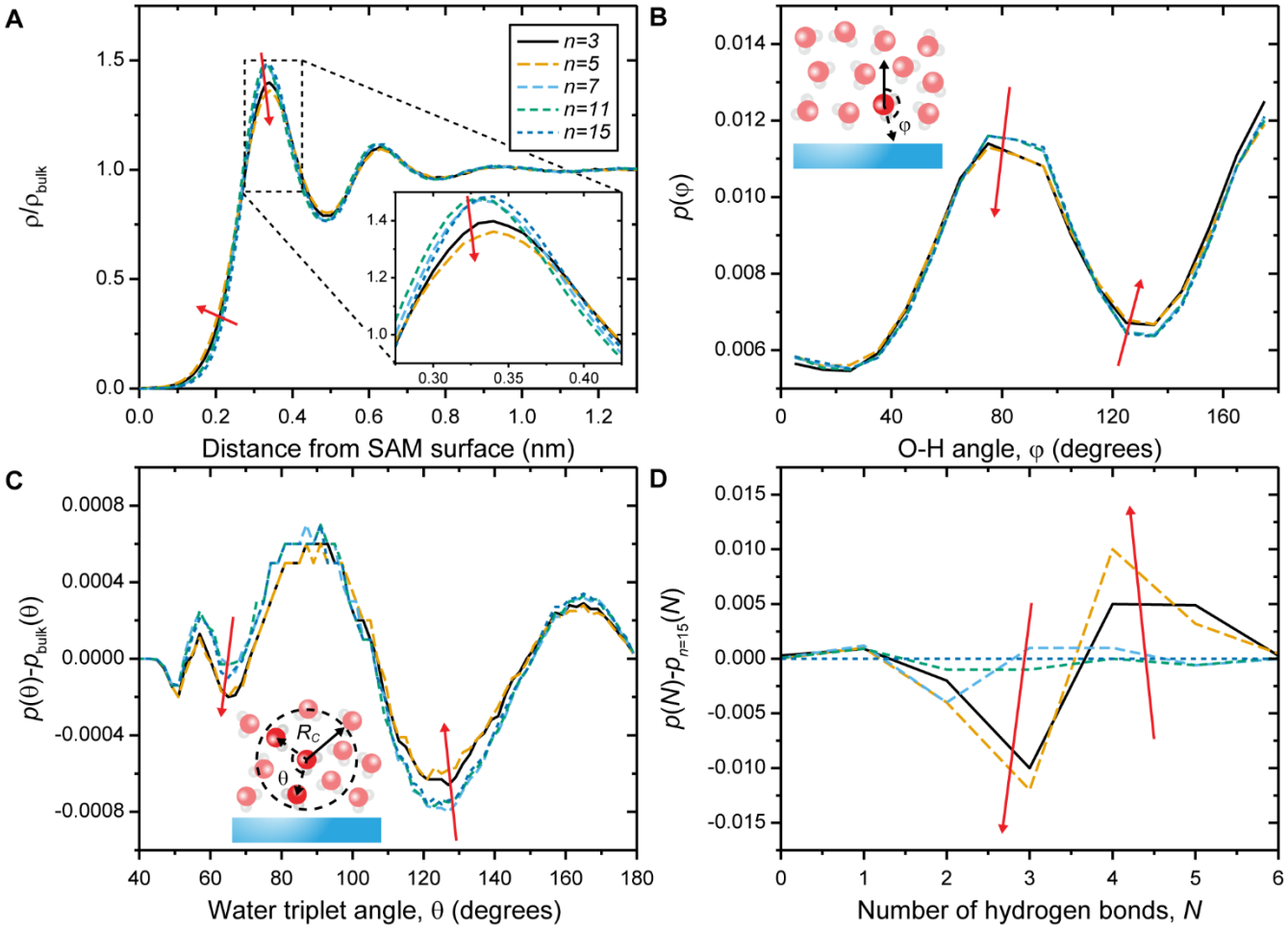

Figure 4. Order parameters measuring interfacial water structure. Red arrows in all figures show changes with decreasing ligand chain length. (A) Water density normalized by bulk water density as a function of distance from the SAM surface. (B) Probability distribution of the angle (φ) formed between water molecule O-H bond vectors and a vector normal to the SAM surface. (C) Probability distribution of the triplet angle (θ) formed by a water molecule with its two nearest neighbors minus the probability distribution of triplet angles formed in bulk water. (D) Probability distribution of the number of hydrogen bonds, *N*, per interfacial water molecule minus the probability distribution for a reference ordered surface ($p_{n=15}(N)$).

neighboring water molecules within a cutoff distance of 3.3 Å as illustrated by the inset in Figure 4C. This parameter has been used to determine structure in bulk water at different temperatures and around solvated peptides.[26, 61, 64] In the bulk water triplet angle distribution, there is a broad primary peak at approximately 100° indicating a preference toward tetrahedral water structure, while the distribution for a Lennard-Jones fluid that lacks directional hydrogen bonding is dominated by a population at 60°.[26, 64] The bulk water distribution is subtracted from the interfacial water distributions in Figure 4C to more easily distinguish these relevant features. Water near each SAM exhibits a lower preference for tetrahedral ordering than bulk water, agreeing with conventional models for water structure near extended nonpolar interfaces.[26] There is a small decrease to the population of θ at approximately 60° for disordered SAMs relative to ordered SAMs that may be attributed to more orientational degrees of freedom for the interfacial water molecules. There is also a slight enhancement to the population of θ at approximately 110°-120° for the disordered SAMs relative to the ordered SAMs, suggesting that there is an increase in tetrahedral ordering for the interfacial water molecules consistent with the increased tetrahedral ordering of water molecules around small nonpolar solutes.

Figure 4D shows the probability distribution for the number of hydrogen bonds formed per interfacial water molecule. A hydrogen bond is counted if the distance between two water oxygen atoms is less than 3.5 Å and the HOO (donor, oxygen, acceptor) angle is less than 30°.[65-66] The difference between the probability distribution for each SAM and the probability distribution for the *n*=15 SAM (a reference ordered SAM) is presented to highlight the differences between ordered and disordered SAMs. Water molecules near the disordered SAM surfaces form four hydrogen bonds approximately 1% more frequently than the water molecules near the ordered SAM surfaces. To compensate, the water molecules near ordered SAMs form three hydrogen bonds approximately 1% more often than the water molecules near disordered SAMs. These results indicate increased hydrogen bonding between water molecules near disordered SAMs that is consistent with the increased tetrahedrality demonstrated by the prior two order parameters.

While the differences in water structure between the disordered and ordered SAMs are small for each of these parameters, these differences are consistent with increased water structure at disordered interfaces for all four parameters. Moreover, the small magnitude of these effects is expected. For example, Giovambattista *et al.* measured the probability distribution of φ as a function of increasing substrate hydrophilicity by tuning a "hydrophilicity parameter" between 0.0 (hydrophobic) and 1.0 (hydrophilic). By changing the hydrophilic parameter from 0.0 to 0.2, they observed only a small shift (approximately 10% difference) in the distribution. They only observed a large shift in the distribution upon increasing the hydrophilic parameter to 0.4 (*i.e.*, inducing a large change to surface polarity).[60] Similarly, Stock *et al.* reported shifts on the order of 10^{-4} in the triplet angle distribution when replacing the number of hydrophilic side chains (glycine and serine) with hydrophobic side chains (leucine) on a model peptide.[26] These two examples suggest that even large changes to surface polarity may result in small changes to the interfacial water structure. Similarly, the small change in water structure measured in Figure 4 results in a significant, two-fold increase in the hydrophobic force between ordered SAMs relative to the hydrophobic force between disordered SAMs (Figure 3), consistent with an effective change in surface polarity. We conclude that disordered SAMs deviate from the conventional behavior of idealized, extended hydrophobic surfaces by increasing local water structure relative to ordered SAMs, thereby decreasing the effective SAM hydrophobicity in accordance with the conventional picture of small length scale hydrophobicity.

Temperature dependence of hydrophobic interactions.

The simulation prediction that interfacial water molecules are more structured near disordered SAM surfaces suggests that a difference in the solvation entropy between disordered and ordered SAM surfaces should be observed. The solvation entropy can be related to the solvation free energy, ΔG_{solv}, by:

$$\Delta S_{\mathrm{solv}} = -\left(\frac{\partial \Delta G_{\mathrm{solv}}}{\partial T}\right)_P \quad (1)$$

We investigated this hypothesis by measuring temperature variations in the hydrophobic force using both simulations and experiments and assuming that the solvation entropy can be related to the slope of the

hydrophobic force versus temperature (see related discussion in the Supporting Information); specifically, we hypothesized that the slope of the hydrophobic force versus temperature would be more positive for disordered SAMs than ordered SAMs given the sign convention that positive hydrophobic forces are attractive.

Figure 5A shows the hydrophobic force measured computationally as a function of temperature for representative disordered SAMs (n=3, n=5, and n=11, unsaturated) and representative ordered SAMs (n=7 and n=11) following the techniques in SI Section S1. We confirmed that SAM order and molecular fluctuations remained constant over the desired temperature range, indicating that the change in the hydrophobic force with temperature may be attributed to the solvation entropy and not to changes in SAM properties (Figure S11). The slopes of the disordered SAM surfaces are positive, indicating that these surfaces become more hydrophobic with increasing temperature. In contrast, the slope of the ordered SAM surface is negative, suggesting that the ordered surface becomes slightly less hydrophobic with increasing temperature. From the slopes of the hydrophobic force versus temperature curves, we infer the relative solvation entropies of the surfaces as:

$$\Delta S_{\mathrm{solv}}^{n=3} < \Delta S_{\mathrm{solv}}^{n=5} < \Delta S_{\mathrm{solv}}^{n=11,\mathrm{unsat.}} < \Delta S_{\mathrm{solv}}^{n=7} < \Delta S_{\mathrm{solv}}^{n=11}. \quad (2)$$

This trend indicates that the solvation entropy increases with increasing SAM order (Figure 2) as expected.[34]

The observed positive slope for disordered SAMs seems to contradict theoretical predictions for large nonpolar solutes, which become less hydrophobic with increasing temperature[34]. However, this result is consistent with prior computational studies measuring the interactions between two graphene plates in water as a function of temperature[31, 67]. The discrepancy with the simulations may be attributed to the selection of water model; while modified TIP3P water accurately reproduces hydration free energies, the model does not fully reproduce the tetrahedral-like structure of water at ambient conditions.[68] However, we emphasize that our goal is to determine how SAM order perturbs interfacial water structure, and thus the finding that the solvation entropy for disordered SAMs is less than the solvation entropy for ordered SAMs is consistent with the measurements of water structure (Figure 4) and supports our hypotheses.

Figure 5B shows the hydrophobic force measured experimentally as a function of temperature for four SAMs ranging from short to long ligand chain lengths and one SAM containing unsaturated ligands. Hydrophobic forces were measured as described previously[41-43] and summarized in SI Section S4. Complete experimental results, including adhesion forces measured in aqueous TEA and methanol and confirmation of temperature reversibility, are provided in SI Section S5. The hydrophobic force decreases linearly with increasing temperature for each of the SAM surfaces, indicating that surfaces become less hydrophobic with increasing temperature. Stock *et al* observed the same temperature dependence trend in the hydrophobic force between n=11 SAMs.[69] Both results are in agreement with the behavior expected of large nonpolar solutes.[34] The slope of the hydrophobic force versus temperature decreases with increasing SAM order, again consistent with the simulation measurements of water structure and the simulated hydrophobic forces. Moreover, SAMs with similar order (measured in Figure 2B) have similar slopes; for example, the slopes of the n=15 and n=17 SAMs are statistically indistinguishable, as are the slopes of the n=11 and unsaturated n=17 SAMs.

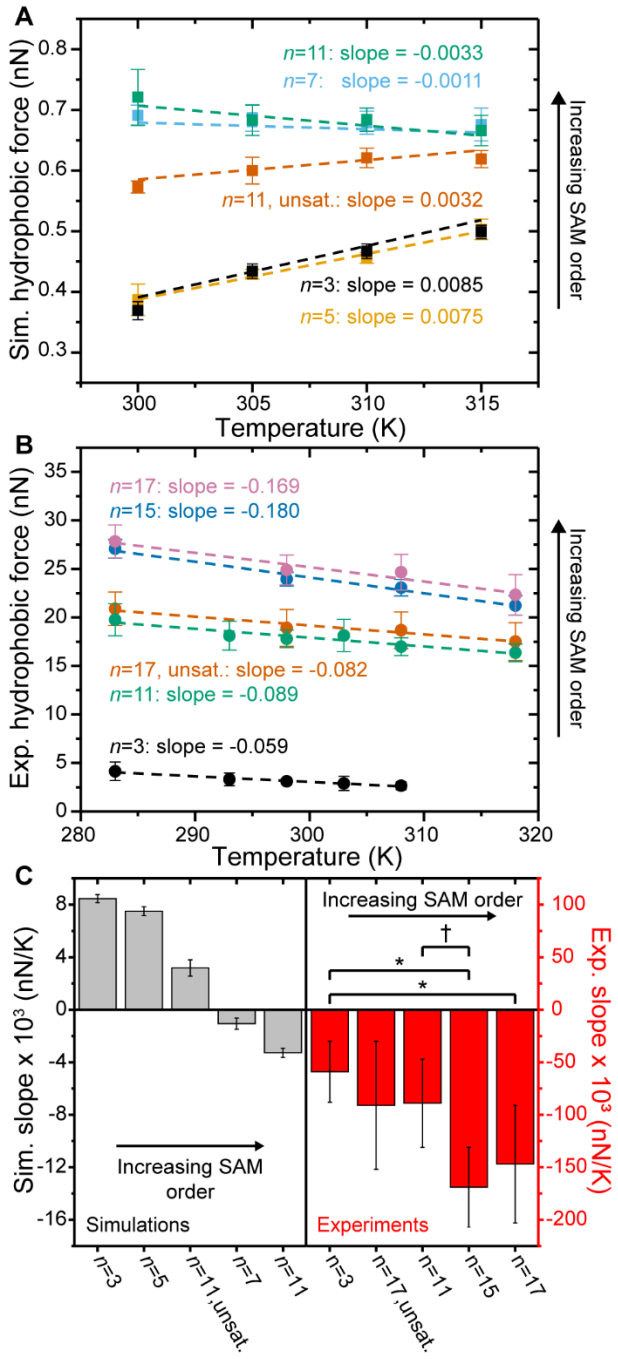

Figure 5. Temperature dependence of the hydrophobic force between alkanethiol SAMs measured from (A) MD simulations and (B) AFM experiments. Error bars in (A) were calculated as in Figure 3B. Error bars not seen are smaller than the symbols. The hydrophobic force data was fit for each independent simulation and experiment (dashed lines) and slopes are reported in the corresponding color. (C) Slope of the hydrophobic force versus temperature for SAMs of increasing order from both simulations and experiments. Error bars in (C) report the standard error of the linear fit to the data (SI Section S5). The asterisk (*) and dagger (†) symbols indicate values are statistically significant with a *p*-value less than 0.05 and 0.1, respectively. The black arrow in each figure indicates the direction of increasing SAM order.

The statistical significance between all the slopes should be noted. We provide a detailed discussion of our statistical analysis in SI Section S5. From this analysis, only the difference between the n=3 and n=17 slopes and between the n=3 and n=15 slopes are statistically significant at a significance level of 95%; however, we do note that the qualitative trend in the slopes with respect to changes in ligand order agrees with expectations. Overall, the combined experimental and simulation results support the hypothesis that *increasing* SAM order *decreases* interfacial water structure and thus *increases* the solvation entropy, leading to similar temperature-dependent hydrophobic interactions between SAMs with similar molecular-scale order. Figure 5C compares trends in the slopes calculated from simulations and experiments to emphasize that similar trends are observed in both sets of measurements. These findings are consistent with the conventional description of length-scale dependent hydrophobic interactions; here, we find that disordered SAMs exhibit signatures of small-length-scale hydrophobicity. These principal findings are summarized schematically in Figure 6.

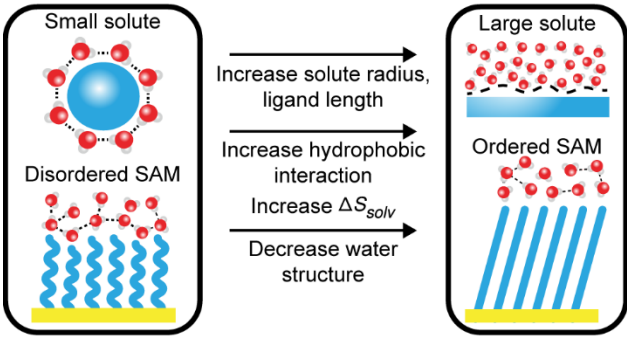

Figure 6. Representation of key results from MD simulations and experiments. Increasing SAM order has a similar effect on hydrophobic interactions, the solvation entropy, and interfacial water structure as increasing the radius of an idealized nonpolar solute.

Conclusions

We performed a joint simulation and experimental study of hydrophobic interactions between nonpolar SAM surfaces. We report two key findings. First, we use atomistic molecular dynamics simulations to show that water molecules at disordered SAM interfaces are slightly more structured than water molecules at ordered SAM interfaces. While the change in interfacial water structure is small, there is a significant, two-fold increase in the magnitude of the hydrophobic force from disordered to ordered SAMs. This finding explains why disordered SAM surfaces appear less hydrophobic than ordered SAM surfaces, despite the materials containing the same chemical identity and surface area. Second, we find that the increased water structure near the disordered SAM surfaces results in a perturbation to the temperature dependence of the hydrophobic interactions. By measuring hydrophobic forces as a function of temperature using both simulations and experiments, we determined that the solvation entropy of disordered SAMs was less than the solvation entropy of ordered SAMs. Both findings are consistent and reveal that hydrophobic interactions at extended nonpolar interfaces sensitively depend on SAM physical properties that disrupt interfacial water structure.

Our results suggest that material selection (*e.g.*, ligand chain length and saturation) can be used to tune the temperature response of hydrophobic interactions between nonpolar materials. This insight could be valuable for the design of synthetic materials, such as responsive colloidal assemblies that assemble or dissemble based on temperature-dependent hydrophobic interactions. This study also raises the question of what other physical parameters may be adjusted to tune hydrophobic interactions. For example, does changing an intrinsically rigid domain of a protein to a flexible, fluctuating domain or introducing substrate curvature to manipulate SAM free volume manipulate the hydrophobicity of the material? Future work will explore the effect of other material parameters on interfacial hydrophobicity, and moreover determine how physical and chemical properties may work in concert to affect the magnitude of hydrophobic interactions at complex interfaces.[41-42]

Acknowledgements

The authors gratefully acknowledge partial support of this research through the University of Wisconsin Materials Research Science and Engineering Center (DMR-1720415). NLA acknowledges support for experiments by the Army Research Office (W911NF-16-1-0154 and W911NF-17-1-0575). RVL and NLA acknowledge support from the Department of Chemical and Biological Engineering of the University of Wisconsin-Madison. This work used the Extreme Science and Engineering Discovery Environment (XSEDE), which is supported by National Science Foundation grant number ACI-1549562.

Supporting Information

Details on simulation preparation and workflows; convergence of simulation measurables; detailed experimental methods; discussion of statistical analysis; discussion of solvation free energies.

References

1. Dill, K. A., Dominant forces in protein folding. *Biochemistry* **1990,** *29* (31), 7133-55.
2. Nicholls, A.; Sharp, K. A.; Honig, B., Protein folding and association: insights from the interfacial and thermodynamic properties of hydrocarbons. *Proteins* **1991,** *11* (4), 281-96.
3. Dobson, C. M., Protein folding and misfolding. *Nature* **2003,** *426* (6968), 884-90.
4. Sanchez-Iglesias, A.; Grzelczak, M.; Altantzis, T.; Goris, B.; Perez-Juste, J.; Bals, S.; Van Tendeloo, G.; Donaldson, S. H., Jr.; Chmelka, B. F.; Israelachvili, J. N.; Liz-Marzan, L. M., Hydrophobic interactions modulate self-assembly of nanoparticles. *ACS Nano* **2012,** *6* (12), 11059-65.
5. Van Lehn, R. C.; Alexander-Katz, A., Ligand-mediated short-range attraction drives aggregation of charged monolayer-protected gold nanoparticles. *Langmuir* **2013,** *29* (28), 8788-98.
6. Beal, R. E.; Toscano-Cantaffa, D.; Young, P.; Rechsteiner, M.; Pickart, C. M., The Hydrophobic Effect Contributes to Polyubiquitin Chain Recognition†. *Biochemistry* **1998,** *37* (9), 2925-2934.
7. Snyder, P. W.; Mecinovic, J.; Moustakas, D. T.; Thomas, S. W., 3rd; Harder, M.; Mack, E. T.; Lockett, M. R.; Heroux, A.; Sherman, W.; Whitesides, G. M., Mechanism of the hydrophobic effect in the biomolecular recognition of arylsulfonamides by carbonic anhydrase. *Proc Natl Acad Sci U S A* **2011,** *108* (44), 17889-94.
8. Friesner, R. A.; Murphy, R. B.; Repasky, M. P.; Frye, L. L.; Greenwood, J. R.; Halgren, T. A.; Sanschagrin, P. C.; Mainz, D. T., Extra precision glide: docking and scoring incorporating a model of hydrophobic enclosure for protein-ligand complexes. *J Med Chem* **2006,** *49* (21), 6177-96.
9. Young, T.; Abel, R.; Kim, B.; Berne, B. J.; Friesner, R. A., Motifs for molecular recognition exploiting hydrophobic enclosure in protein-ligand binding. *Proc Natl Acad Sci U S A* **2007,** *104* (3), 808-13.
10. Tilton, R. D.; Robertson, C. R.; Gast, A. P., Manipulation of hydrophobic interactions in protein adsorption. *Langmuir* **1991,** *7* (11), 2710-2718.
11. Nakanishi, K.; Sakiyama, T.; Imamura, K., On the adsorption of proteins on solid surfaces, a common but very complicated phenomenon. *Journal of Bioscience and Bioengineering* **2001,** *91* (3), 233-244.
12. Van Lehn, R. C.; Atukorale, P. U.; Carney, R. P.; Yang, Y. S.; Stellacci, F.; Irvine, D. J.; Alexander-Katz, A., Effect of particle diameter and surface composition on the spontaneous fusion of monolayer-protected gold nanoparticles with lipid bilayers. *Nano Lett* **2013,** *13* (9), 4060-7.
13. Van Lehn, R. C.; Alexander-Katz, A., Pathway for insertion of amphiphilic nanoparticles into defect-free lipid bilayers from atomistic molecular dynamics simulations. *Soft Matter* **2015,** *11* (16), 3165-75.
14. Lum, K.; Chandler, D.; Weeks, J. D., Hydrophobicity at Small and Large Length Scales. *The Journal of Physical Chemistry B* **1999,** *103* (22), 4570-4577.
15. Huang, D. M.; Geissler, P. L.; Chandler, D., Scaling of Hydrophobic Solvation Free Energies. *The Journal of Physical Chemistry B* **2001,** *105* (28), 6704-6709.
16. Chandler, D., Interfaces and the driving force of hydrophobic assembly. *Nature* **2005,** *437* (7059), 640-7.
17. Daidone, I.; Ulmschneider, M. B.; Di Nola, A.; Amadei, A.; Smith, J. C., Dehydration-driven solvent exposure of hydrophobic surfaces as a driving force in peptide folding. *Proc Natl Acad Sci U S A* **2007,** *104* (39), 15230-5.
18. Godawat, R.; Jamadagni, S. N.; Garde, S., Characterizing hydrophobicity of interfaces by using cavity formation, solute binding, and water correlations. *Proc Natl Acad Sci U S A* **2009,** *106* (36), 15119-24.
19. Acharya, H.; Vembanur, S.; Jamadagni, S. N.; Garde, S., Mapping hydrophobicity at the nanoscale: Applications to heterogeneous surfaces and proteins. *Faraday Discussions* **2010,** *146*.
20. Patel, A. J.; Varilly, P.; Jamadagni, S. N.; Acharya, H.; Garde, S.; Chandler, D., Extended surfaces modulate hydrophobic interactions of neighboring solutes. *Proc Natl Acad Sci U S A* **2011,** *108* (43), 17678-83.

21. Harris, R. C.; Pettitt, B. M., Effects of geometry and chemistry on hydrophobic solvation. *Proc Natl Acad Sci U S A* **2014,** *111* (41), 14681-6.
22. Patel, A. J.; Varilly, P.; Jamadagni, S. N.; Hagan, M. F.; Chandler, D.; Garde, S., Sitting at the edge: how biomolecules use hydrophobicity to tune their interactions and function. *J Phys Chem B* **2012,** *116* (8), 2498-503.
23. Willard, A. P.; Chandler, D., The molecular structure of the interface between water and a hydrophobic substrate is liquid-vapor like. *J Chem Phys* **2014,** *141* (18), 18C519.
24. Remsing, R. C.; Xi, E.; Vembanur, S.; Sharma, S.; Debenedetti, P. G.; Garde, S.; Patel, A. J., Pathways to dewetting in hydrophobic confinement. *Proc Natl Acad Sci U S A* **2015,** *112* (27), 8181-6.
25. Vaikuntanathan, S.; Rotskoff, G.; Hudson, A.; Geissler, P. L., Necessity of capillary modes in a minimal model of nanoscale hydrophobic solvation. *Proc Natl Acad Sci U S A* **2016,** *113* (16), E2224-30.
26. Stock, P.; Monroe, J. I.; Utzig, T.; Smith, D. J.; Shell, M. S.; Valtiner, M., Unraveling Hydrophobic Interactions at the Molecular Scale Using Force Spectroscopy and Molecular Dynamics Simulations. *ACS Nano* **2017,** *11* (3), 2586-2597.
27. Kanduc, M.; Netz, R. R., From hydration repulsion to dry adhesion between asymmetric hydrophilic and hydrophobic surfaces. *Proc Natl Acad Sci U S A* **2015,** *112* (40), 12338-43.
28. Giovambattista, N.; Lopez, C. F.; Rossky, P. J.; Debenedetti, P. G., Hydrophobicity of protein surfaces: Separating geometry from chemistry. *Proc Natl Acad Sci U S A* **2008,** *105* (7), 2274-9.
29. Altabet, Y. E.; Haji-Akbari, A.; Debenedetti, P. G., Effect of material flexibility on the thermodynamics and kinetics of hydrophobically induced evaporation of water. *Proc Natl Acad Sci U S A* **2017,** *114* (13), E2548-E2555.
30. Ben-Amotz, D., Water-Mediated Hydrophobic Interactions. *Annu Rev Phys Chem* **2016,** *67*, 617-38.
31. Zangi, R.; Berne, B. J., Temperature dependence of dimerization and dewetting of large-scale hydrophobes: a molecular dynamics study. *J Phys Chem B* **2008,** *112* (29), 8634-44.
32. Shin, S.; Willard, A. P., Characterizing Hydration Properties Based on the Orientational Structure of Interfacial Water Molecules. *J Chem Theory Comput* **2018,** *14* (2), 461-465.
33. Shin, S.; Willard, A. P., Water's Interfacial Hydrogen Bonding Structure Reveals the Effective Strength of Surface-Water Interactions. *J Phys Chem B* **2018,** *122* (26), 6781-6789.
34. Huang, D. M.; Chandler, D., Temperature and length scale dependence of hydrophobic effects and their possible implications for protein folding. *Proc Natl Acad Sci U S A* **2000,** *97* (15), 8324-7.
35. Chothia, C., Hydrophobic bonding and accessible surface area in proteins. *Nature* **1974,** *248* (5446), 338-339.
36. Ulmschneider, M. B.; Ulmschneider, J. P.; Schiller, N.; Wallace, B. A.; von Heijne, G.; White, S. H., Spontaneous transmembrane helix insertion thermodynamically mimics translocon-guided insertion. *Nat Commun* **2014,** *5*, 4863.
37. Ojemalm, K.; Higuchi, T.; Jiang, Y.; Langel, U.; Nilsson, I.; White, S. H.; Suga, H.; von Heijne, G., Apolar surface area determines the efficiency of translocon-mediated membrane-protein integration into the endoplasmic reticulum. *Proc Natl Acad Sci U S A* **2011,** *108* (31), E359-64.
38. Durham, E.; Dorr, B.; Woetzel, N.; Staritzbichler, R.; Meiler, J., Solvent accessible surface area approximations for rapid and accurate protein structure prediction. *J Mol Model* **2009,** *15* (9), 1093-108.
39. Chen, S.; Itoh, Y.; Masuda, T.; Shimizu, S.; Zhao, J.; Ma, J.; Nakamura, S.; Okuro, K.; Noguchi, H.; Uosaki, K.; Aida, T., Ionic interactions. Subnanoscale hydrophobic modulation of salt bridges in aqueous media. *Science* **2015,** *348* (6234), 555-9.
40. Huang, K.; Gast, S.; Ma, C. D.; Abbott, N. L.; Szlufarska, I., Comparison between Free and Immobilized Ion Effects on Hydrophobic Interactions: A Molecular Dynamics Study. *J Phys Chem B* **2015,** *119* (41), 13152-9.
41. Ma, C. D.; Wang, C.; Acevedo-Velez, C.; Gellman, S. H.; Abbott, N. L., Modulation of hydrophobic interactions by proximally immobilized ions. *Nature* **2015,** *517* (7534), 347-50.

42. Wang, C.; Ma, C. D.; Yeon, H.; Wang, X.; Gellman, S. H.; Abbott, N. L., Nonadditive Interactions Mediated by Water at Chemically Heterogeneous Surfaces: Nonionic Polar Groups and Hydrophobic Interactions. *J Am Chem Soc* **2017,** *139* (51), 18536-18544.
43. Yeon, H.; Wang, C.; Van Lehn, R. C.; Abbott, N. L., Influence of Order within Nonpolar Monolayers on Hydrophobic Interactions. *Langmuir* **2017,** *33* (19), 4628-4637.
44. Cui, X.; Liu, J.; Xie, L.; Huang, J.; Liu, Q.; Israelachvili, J.; Zeng, H., Modulation of Hydrophobic Interaction by Mediating Surface Nanoscale Structure and Chemistry, not Monotonically by Hydrophobicity. *Angew Chem Int Ed Engl* **2018**.
45. Love, J. C.; Estroff, L. A.; Kriebel, J. K.; Nuzzo, R. G.; Whitesides, G. M., Self-assembled monolayers of thiolates on metals as a form of nanotechnology. *Chem Rev* **2005,** *105* (4), 1103-69.
46. Siu, S. W.; Pluhackova, K.; Bockmann, R. A., Optimization of the OPLS-AA Force Field for Long Hydrocarbons. *J Chem Theory Comput* **2012,** *8* (4), 1459-70.
47. Sun, Y.; Kollman, P. A., Hydrophobic solvation of methane and nonbond parameters of the TIP3P water model. *Journal of Computational Chemistry* **1995,** *16* (9), 1164-1169.
48. Abraham, M. J.; Murtola, T.; Schulz, R.; Páll, S.; Smith, J. C.; Hess, B.; Lindahl, E., GROMACS: High performance molecular simulations through multi-level parallelism from laptops to supercomputers. *SoftwareX* **2015,** *1-2*, 19-25.
49. Parrinello, M.; Rahman, A., Polymorphic transitions in single crystals: A new molecular dynamics method. *Journal of Applied Physics* **1981,** *52* (12), 7182-7190.
50. Bussi, G.; Donadio, D.; Parrinello, M., Canonical sampling through velocity rescaling. *J Chem Phys* **2007,** *126* (1), 014101.
51. Roux, B., The calculation of the potential of mean force using computer simulations. *Computer Physics Communications* **1995,** *91* (1-3), 275-282.
52. Hub, J. S.; de Groot, B. L.; van der Spoel, D., g_wham—A Free Weighted Histogram Analysis Implementation Including Robust Error and Autocorrelation Estimates. *Journal of Chemical Theory and Computation* **2010,** *6* (12), 3713-3720.
53. Gojzewski, H.; Kappl, M.; Ptak, A., Effect of the Chain Length and Temperature on the Adhesive Properties of Alkanethiol Self-Assembled Monolayers. *Langmuir* **2017,** *33* (43), 11862-11868.
54. Hofsäß, C.; Lindahl, E.; Edholm, O., Molecular Dynamics Simulations of Phospholipid Bilayers with Cholesterol. *Biophysical Journal* **2003,** *84* (4), 2192-2206.
55. Ramin, L.; Jabbarzadeh, A., Odd-even effects on the structure, stability, and phase transition of alkanethiol self-assembled monolayers. *Langmuir* **2011,** *27* (16), 9748-59.
56. Castillo, J. M.; Klos, M.; Jacobs, K.; Horsch, M.; Hasse, H., Characterization of alkylsilane self-assembled monolayers by molecular simulation. *Langmuir* **2015,** *31* (9), 2630-8.
57. Porter, M. D.; Bright, T. B.; Allara, D. L.; Chidsey, C. E. D., Spontaneously organized molecular assemblies. 4. Structural characterization of n-alkyl thiol monolayers on gold by optical ellipsometry, infrared spectroscopy, and electrochemistry. *Journal of the American Chemical Society* **1987,** *109* (12), 3559-3568.
58. Miller, W. J.; Abbott, N. L., Influence of van der Waals Forces from Metallic Substrates on Fluids Supported on Self-Assembled Monolayers Formed from Alkanethiols. *Langmuir* **1997,** *13* (26), 7106-7114.
59. Lee, C. Y.; McCammon, J. A.; Rossky, P. J., The structure of liquid water at an extended hydrophobic surface. *The Journal of Chemical Physics* **1984,** *80* (9), 4448-4455.
60. Giovambattista, N.; Debenedetti, P. G.; Rossky, P. J., Effect of surface polarity on water contact angle and interfacial hydration structure. *J Phys Chem B* **2007,** *111* (32), 9581-7.
61. Head-Gordon, T.; Stillinger, F. H., An orientational perturbation theory for pure liquid water. *The Journal of Chemical Physics* **1993,** *98* (4), 3313-3327.
62. Chaimovich, A.; Shell, M. S., Tetrahedrality and structural order for hydrophobic interactions in a coarse-grained water model. *Phys Rev E Stat Nonlin Soft Matter Phys* **2014,** *89* (2), 022140.
63. Xiao, S.; Figge, F.; Stirnemann, G.; Laage, D.; McGuire, J. A., Orientational Dynamics of Water at an Extended Hydrophobic Interface. *J Am Chem Soc* **2016,** *138* (17), 5551-60.

64. Lynden-bell, R. M.; Head-gordon, T., Solvation in modified water models: towards understanding hydrophobic effects. *Molecular Physics* **2006,** *104* (22-24), 3593-3605.
65. Luzar, A.; Chandler, D., Structure and hydrogen bond dynamics of water–dimethyl sulfoxide mixtures by computer simulations. *The Journal of Chemical Physics* **1993,** *98* (10), 8160-8173.
66. Luzar, A.; Chandler, D., Hydrogen-bond kinetics in liquid water. *Nature* **1996,** *379* (6560), 55-57.
67. Graziano, G., Dimerization thermodynamics of large hydrophobic plates: a scaled particle theory study. *J Phys Chem B* **2009,** *113* (32), 11232-9.
68. Agarwal, M.; Kushwaha, H. R.; Chakravarty, C., Local order, energy, and mobility of water molecules in the hydration shell of small peptides. *J Phys Chem B* **2010,** *114* (1), 651-9.
69. Stock, P.; Utzig, T.; Valtiner, M., Direct and quantitative AFM measurements of the concentration and temperature dependence of the hydrophobic force law at nanoscopic contacts. *J Colloid Interface Sci* **2015,** *446*, 244-51.